Neurite orientation dispersion and density imaging can detect presymptomatic axonal degeneration in the spinal cord of ALS mice

Rodolfo G. Gatto, MD, PhD[a]
Sourajit M. Mustafi, PhD[b]
Manish Y. Amin, MS[c]
Thomas H. Mareci, PhD[d]
Yu-Chien Wu, PhD[b]
Richard L. Magin, PhD[e]

[a] Department of Anatomy and Cell Biology, University of Illinois at Chicago, Chicago, IL, USA
[b] Department of Radiology and Imaging Sciences, Indiana University, School of Medicine Indianapolis, IN, USA
[c] Department of Physics, University of Florida, Gainesville, FL, USA
[d] Department of Biochemistry and Molecular Biology, University of Florida, Gainesville, FL, USA
[e] Department of Bioengineering, University of Illinois at Chicago, Chicago, IL, USA

Correspondence to: Rodolfo G. Gatto
E-mail: rodogatto@gmail.com

Summary

Neurite orientation dispersion and density imaging (NODDI), a MRI multi-shell diffusion technique, has offered new insights for the study of microstructural changes in neurodegenerative diseases. Mainly, the present study aimed to determine the connection between NODDI-derived parameters and changes in white matter (WM) abnormalities at early stages of amyotrophic lateral sclerosis (ALS). Spinal cords from ALS mice (G93A-SOD1 mice) were scanned in a Bruker Avance III HD 17.6T magnet. Fluorescent axonal-tagged mice (YFP, G93A-SOD1 mice) were used for quantitative histological analysis. NODDI showed a decrease in intra-cellular volume fraction (-24%) and increases in orientation dispersion index (+35%) and isotropic volume fraction (+33%). In addition, histopathological results demonstrated a reductions in axonal area (-11%) and myelin content (-29%). A histological decrease in WM intra-axonal space (-71%) and an increase in the extra-axonal compartment (+22%) were also detected. Our studies demonstrate that NODDI may be a suitable technique for detecting presymptomatic spinal cord WM microstructural degeneration in ALS.

KEY WORDS: amyotrophic lateral sclerosis, axonal degeneration, G93A-SOD1 mice, neurite orientation and density imaging, spinal cord, yellow fluorescent protein.

Introduction

Amyotrophic lateral sclerosis (ALS) is a neurodegenerative disease characterized by a progressive onset and loss of locomotor symptoms, leading to a rapid functional deterioration and premature death (Wijesekera and Leigh, 2009). Classical neuropathological studies and neurophysiological evidence have linked this disease to early degeneration of motor neurons located in the spinal cord (SC). The vast majority of patients with ALS develop this disease as a spontaneous mutation form (sporadic ALS), while a small proportion of ALS individuals develop a familial inherited form (FALS) (Orsini et al., 2015). One of the first genetic alterations to be characterized in FALS was a mutation in the superoxide dismutase gene, and this event led to the development of the transgenic G93A-SOD1 mouse, which is among the classic animal models used in ALS research (Gurney, 1994). In view of the predominance of the spontaneous form of ALS and the short time frame between disease onset and death, a non-invasive technique able to detect the disease in the early stages and monitor the progress of treatments would be desirable. The fast acquisition time and non-invasive profile of MRI have made it one of the imaging techniques of choice for the detection and evaluation of various diseases affecting the central nervous system (CNS) (Gatto et al., 2015a; Magin, 2017). Among different structural MRI techniques, diffusion tensor imaging (DTI) has been found to be one of the most useful methods for unveiling microstructural changes in brain white matter (WM) (Alexander et al., 2007). Although DTI has demonstrated sensitivity to early changes in the SC tissue microstructure in subjects with ALS (Nair et al., 2010), this technique uses a single-tensor diffusion model. This is a limiting factor from the perspective of the characterization of heterogeneous microstructures in brain tissues and the representation of important pathological features of ALS. Thus, considering the complex processes that occur across different cell populations during the early development of this disease, new approaches including multiple diffusion compartments have been proposed to provide more information about the underlying neuropathology (Kaden et al., 2016). Among the different multi-compartment MRI diffusion models, neurite orientation dispersion and density imaging (NODDI) has recently offered new insights into complex microstructural changes in WM (Sato et al., 2017).

In NODDI, the diffusion signal is decomposed into three different compartments: 1) a restricted compartment – anisotropic Gaussian diffusion with zero radial diffusivity – referred to as the intra-neurite space; 2) a hindered compartment – anisotropic Gaussian diffusion with non-zero radial diffusivity related to neurite density via the tortuosity model – referred to as the extra-neurite space; and 3) free water – isotropic Gaussian diffusion – i.e.

cerebrospinal fluid (CSF) or other free water. Although this technique has been applied in different neurodegenerative diseases (Colgan et al., 2016; Kamagata et al., 2016; Kodiweera et al., 2016; By et al., 2017; Granberg et al., 2017; Schneider et al., 2017a; Slattery et al., 2017) and other neuropathological conditions (Adluru et al., 2014; Winston et al., 2014; Timmers et al., 2015; Wen et al., 2015; Kini et al., 2016; Irie et al., 2017; Song et al., 2017; Crombe et al., 2018; Wu et al., 2018), it has rarely been implemented for the study of ALS (Jelescu and Budde, 2017).

Extensive biological evidence characterizes ALS as a complex motor neuron disease (Redler and Dokholyan, 2012). However, only a small number of investigations have been able to show the important role of lost axonal connections as one of the key factors present in the early stages of ALS (Morfini et al., 2013). To address this, new in vivo genetic methods have been developed, including new lines of transgenic mice expressing yellow fluorescent proteins (YFPs) in specific cortical neurons (Gatto et al., 2015a,b). By combining these reporters with models of neurodegenerative disease it has been possible to obtain detailed characterization of morphological features of individual neurons and axonal structures visualized in great detail (Gatto et al., 2018 b, c).

While most NODDI diffusion studies are currently focused on the application of this model for detecting and predicting outcomes in different neurodegenerative diseases, there is limited understanding of the basic WM microstructural changes occurring at the earlier (presymptomatic) stages of these diseases. Moreover, only a limited number of studies has correlated imaging biomarkers with microstructural alterations in ALS. To fill this gap in knowledge, the purpose of this study was to determine whether NODDI can detect alterations in axonal connectivity in early ALS stages and to validate the outputs from this model with histological techniques applied in fluorescent axon-labeled ALS mice.

Materials and methods

Theory

Using NODDI it is possible to distinguish three compartments in the brain: 1) the intra-neurite space, modeled as restricted diffusion (a collection of sticks forming a Watson distribution) related to the intra-cellular volume fraction or neurite density index (NDI); 2) the extra-neurite space, modeled as anisotropic Gaussian diffusion related to the extra-cellular volume fraction; and 3) a free water or CSF compartment, modeled as isotropic Gaussian diffusion, also named the isotropic volume fraction (IVF). In addition, from the Watson distribution, NODDI provides information on the orientation dispersion of axons, expressed as the orientation dispersion index (ODI), which quantifies the angular variation of neurite dispersion.

The normalized MRI signal A is represented in equation (1):

$$A = (1 - v_{iso}) (v_{ic} A_{ic} + (1 - v_{ic}) A_{ec}) + v_{iso} A_{iso} \quad (1)$$

where v stands for volume fraction; *ic* for intra-cellular or intra-neurite; *ec* for extra-cellular or extra-neurite; and *iso* for the isotropic CSF compartment (Zhang et al.,

2012). For NODDI fitting, the initial conditions for isotropic free-water diffusivity and the intrinsic diffusivity of the neural tissue were set at 2.0×10^{-3} mm^2/s and 0.6×10^{-3} mm^2/s, respectively, as suggested previously (Kodiweera et al., 2016).

Animal preparation

All procedures used to obtain tissues followed a protocol approved by the Animal Care Committee at the University of Illinois in Chicago. C57BJ6 mice, overexpressing the *SOD1* transgene with the G93A mutation, were obtained from the Jackson Laboratory (JAX, catalog number 004435). The transgenic G93A-SOD1 mouse has been extensively characterized as an animal model for ALS, developing motor symptoms at approximately 110 days of age and dying at around 160 days (Mancuso et al., 2012). Specifically, *ex vivo* spinal cords from ALS mice (G93A-SOD1) and wild-type (WT) littermates at the early (presymptomatic, day 80) and later stages of the disease (symptomatic, day 120) were used for our MRI experiments. For quantitative histological analysis, an additional group of fluorescent axon-labeled mice was bred. Mice encoding a YFP transgene associated with a neuronal Thy1 promoter were chosen to evaluate morphological axonal anomalies (JAX, catalog number 003709). Hence, to visualize neurite structures in ALS mice, we generated double transgenic mice (YFP, G93A-SOD1), while littermates carrying only the fluorescent transgene (YFP) were used as a control group. During the breeding, which complied with animal care protocols, the mice had easy access to food and water and were checked daily to assess their level of well-being and health. In any situation of distress or pain, mice were euthanized in carbon dioxide following standard protocols. A total of 40 animals divided into four groups were used to complete this study (n=6 per group for MRI studies and n=4 per group for histological analysis). Animals were rendered unconscious with CO_2 inhalation, and then transcardiac perfused with a phosphate buffered saline (PBS) and 4% paraformaldehyde (PFA) solution. Serial spine laminectomies were performed and the SCs were extracted intact and then immersed in PFA (> 48 hours). Prior to imaging, the SCs were soaked overnight in PBS to remove the fixative and then placed in individual 5-mm diameter nuclear magnetic resonance spectroscopy (NMR) tubes (New Era, catalog number NEML5-7, 300-400 MHz) filled with fluorocarbon oil (Fluorinert®, 3M, Maplewood, MN). For our first SC experiments, each 5-mm tube (containing a single SC) was positioned in a 5-mm radiofrequency (RF) coil. For our second set of experiments, performed using multiple SCs, each 5-mm NMR tube was initially placed inside a 20-mm diameter NMR tube (New Era, catalog number NE-L25-7) using a custom-made plastic tube holder and then scanned using a 20-mm RF coil. Images were acquired with an ultra-high field 17.6T vertical-bore Avance III scanner, micro-2.5 gradients, and Paravision 6.0 software (Bruker, Karlsruhe, Germany).

Imaging protocol

MRI scans were performed using a Bruker Avance III HD 17.6T 750Hz magnet and micro-2.5 gradients (1500 mT/m) with 5- and 25-mm RF coils. All imaging acquisi-

tion experiments were performed at room temperature (approx. 25°C) and split into two sessions. In an initial session, individual SCs (n=1 per group) were scanned using a 5-mm coil to establish the feasibility of the method to detect presymptomatic changes in ALS mice. Then, using a 25-mm coil, a second set of experiments was performed in which multiple SCs (n=5 per group), were scanned simultaneously, in order to increase the efficiency and reduce variability between measurements.

Individual SCs from the WT and G93A-SOD1 mice (at day 80 and day 120) were placed in NMR tubes and individually scanned overnight (12 hrs) using a 5-mm coil (n=1 SC per group). Scans were centered in the lumbar position of the SC and consisted of seven slices of 0.3 mm thickness located between the third and fifth lumbar segment and perpendicularly aligned to the long axis of the SC (Fig. 1a). A spin echo sequence was used for diffusion-weighted image acquisition with TR/TE 3000/34 msec, a matrix size of 128x128x7, a diffusion pulse length (δ) of 3.5 msec, separation between start of the pulses (Δ) of 17.5 msec, and a field of view (FOV) of 4 mm x 4 mm. Resolution 100x100x300 microns. Five diffusion-weighting shells were used with diffusion weightings of 550, 2974, 3597, 12693 and 12706 s/mm^2, respectively, with 64 directions on each shell. Total acquisition time per SC was 14 hours and 18 minutes.

We acquired new scans using a setting with multiple SCs in a single tube (n=5 SCs per group). An additional 2-mm capillary tube was filled with distilled water as a reference marker (Fig. 3a). For each set of five SCs, a total of 15 axial slices was acquired centered at the lumbar level, oriented along the rostral-caudal axis of each SC. Diffusion-weighted images were acquired using a spin echo sequence with TR/TE 4000/28 msec, interleaved 0.15-mm thick slices, a FOV = 20 x 20 x 3 mm^3 in each block of slices, in-plane acquisition matrix = 133 x 133, for an isotropic image resolution of 150 μm. Diffusion weightings were two b-values at 700 s/mm^2 in 12 directions and 2500 s/mm^2 in 64 directions with a δ of 3.5 msec, a Δ of 17.5 msec. Total scanning time was 24 hours and 12 minutes. Data were analyzed using NODDI algorithms freely available at: http://mig.cs.ucl.ac.uk/index.php?n=Tutorial.NODDImatlab. The output data files from five representative slices were processed using ImageJ toolbox for NIFTY files (Schneider et al., 2012). The WM anterolateral region for manual segmentation and data extraction was based on the early microstructural changes described in our previous studies (Gatto et al., 2018a,b). Output parameters (NDI, ODI and IVF) were extracted for further statistical analysis (Fig.s 1b, 2b).

Histology

After dissection, SCs were placed in progressive solutions of sucrose (5-30%) for an additional 24 hours for cryoprotection. After embedding in optical cutting temperature (OCT) polymer compound (Tissue Tek, Sakura Finetek USA Inc, Torrance, California, U.S.A., catalog number 4583), 50 μm-thick SC sections were obtained using a microtome (Leica cryostat CM 1850 Cryostat, Buffalo Grove, IL). Coronal sections of lumbar SC were used for histological analysis. Each section was mounted on a slide (Fisher Scientific, Hampton, New Hampshire. U.S.A., Fisherbrand Superforst, catalog number
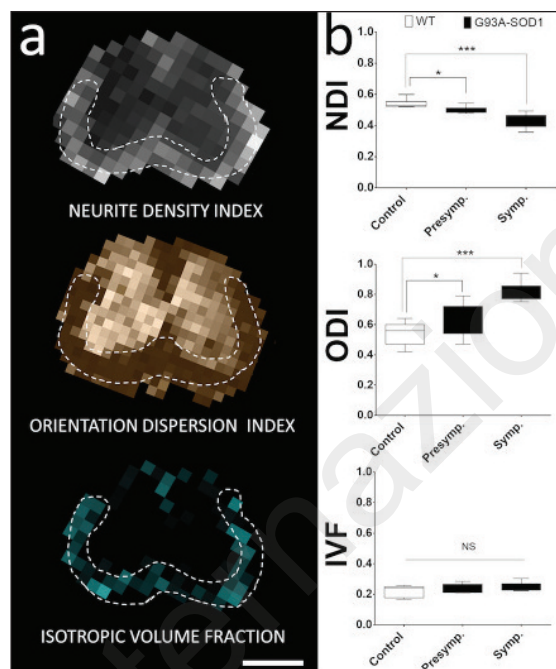

Figure 1 - *Ex vivo* microstructural changes in ALS mice can be detected by neurite orientation and density imaging (NODDI).
a) Axial MRI images showing different NODDI outputs from individual lumbar mice spinal cords. The region of interest taken for data analysis was centered in the anterolateral WM funiculus (white dotted line). b) NODDI data from seven spinal cord segments from WT mice (controls) and G93A-SOD1 mice (ALS mice) at the presymptomatic (day 80) and symptomatic (day 120) stages. Three main parameters from NODDI are analyzed: neurite density index (NDI); orientation dispersion index (ODI) (extra-cellular compartment) and isotropic volume fraction (IVF) representing the free water compartment. (Note that IVF is mostly distributed in the white matter regions). (* p < 0.05), (** p < 0.01), (*** p < 0.01), (n=1 mice per group, 7 axial slices per animal). Scale bar = 1mm.

12-550-15) and dried for 15 minutes. Then, the OCT polymer compound was removed by washing three times with tris base buffer (TBS). Sections were permeabilized with Triton-X100 0.25% for 10 minutes and blocked with 5% goat serum for an hour in TBS. Spinal cord sections were mounted on the slides. Slides were dried and mounted in Vecta-Shield mounting media (Vector Laboratories, Burlingame, CA). Images were acquired with confocal microscopy (ZEISS LSM 710 confocal microscope, ZEISS Microscopy, Germany). SC sections for quantitative analysis were selected using similar anatomical reference and stereotaxic coordinates as used in our MRI studies (Watson et al., 2008). Confocal microscopy images were obtained by background subtraction using negative control samples without primary antibody and collected by two independent channels: a 534 nm channel for the YFP signal and a 647 nm channel to detect fluorescent emission antibodies from other markers. To evaluate the structural status of the neuronal membranes in our preparations, we performed immunohistochemical staining with myelin basic protein (MBP) (PhosphoSolutions®, Aurora, Colorado,

U.S.A., catalog number 1120-MBP, 1:500). Quantitative measures were obtained by mean pixel value using auto-threshold methods. Briefly, the procedure divides the image into objects and background with an initial threshold. Average numbers of pixels at, below or above the threshold were computed and subsequently used per data point. The pixel values of each region of interest were compiled and tabulated for statistical analysis.

Statistical analysis

Data were tabulated and analyzed using GraphPad Prism 6 software (GraphPad Software Inc., La Jolla, California, U.S.A.). Using power analysis calculations and the results of our first experiment and taking into account the nature of each variable, we established the minimum number of animals for each experimental group. For quantitative analysis of NODDI outputs (NDI, ODI, and IVF) and fluorescence levels in cellular markers (YFP and MBP), we used one-way ANOVA and Tukey's post-hoc tests. Values of $p < 0.05$, $p < 0.01$ and $p < 0.001$ were used to demonstrate degrees of statistical significance. Results were replicated by application of non-parametric statistical tools (Mann-Whitney test). Error bars in all the Figures represent standard error of the mean.

Results

To evaluate whether outputs from NODDI can detect presymptomatic microstructural changes, WM was segmented manually from seven axial sections centered in the lumbar anterolateral funiculi of a single SC from each mouse group (Fig. 1a). The compiled data showed that the NDI in the presymptomatic mice (day 80) was significantly lower than in the control mice (WT mice = 0.54 +/- 0.02 *vs* G93A-SOD1 mice = 0.49 +/- 0.02; -9%, $p < 0.05$), and that the same was true in the symptomatic stage (day 120) (WT mice = 0.54 +/- 0.02 *vs* G93A-SOD1 mice = 0.42 +/- 0.03; -22%, $p < 0.001$). In addition, the ODI was significantly higher both in the presymptomatic (day 80) G93A-SOD1 mice compared

with the control mice (WT mice = 0.54 +/- 0.007 *vs* G93A-SOD1 mice = 0.61 +/- 0.04; +17% with $p < 0.05$) and in the symptomatic mice (day 120) (WT mice = 0.54 +/- 0.07 *vs* G93A-SOD1 mice = 0.82 +/- 0.06; +52 %, $p < 0.05$). However, IVF displayed no significant differences between the different groups of mice at any stage (WT mice = 0.22 +/- 0.06 *vs* day 80 G93A-SOD1 mice = 0.23 +/- 0.03 or day 120 G93A-SOD1 mice = 0.25 +/- 0.03, Fig. 1b). Recently, an additional model parameter, isotropic restricted fraction (IrF), was introduced to account for a stationary compartment within the water diffusion in fixed *ex vivo* preparation. Analysis of IrF in our *ex vivo* SC preparations did not show significant differences between SC groups, indicating no significant differences in restricted water diffusion in our preparations (Fig. 2).

Outputs from the second set of studies involving the five SCs-per-tube *ex vivo* measurements (Fig. 3a) demonstrated larger differences in NDI values between WT and presymptomatic G93A-SOD1 mice (WT mice = 0.46 +/- 0.01 *vs* G93A-SOD1 mice = 0.36 +/- 0.01; -24%, $p < 0.001$) and between WT and symptomatic G93A-SOD1 mice (WT mice = 0.45 +/- 0.01 *vs* G93A-SOD1 mice = 0.32 +/- 0.01; -29%, $p < 0.001$). Increased ODI values were observed in presymptomatic mice versus control animals (WT mice = 0.43 +/- 0.06 vs G93A-SOD1 mice = 0.58 +/- 0.03; +35%, $p < 0.01$) and in symptomatic mice *vs* controls (WT mice = 0.42 +/- 0.04 *vs* G93A-SOD1 mice = 0.73 +/- 0.03; +74 %, $p < 0.001$). Particular to this set of experiments in multiple SCs was the finding of a significant increase in IVF in G93A-SOD1 mice versus WT mice at 80 days (WT mice = 0.15 +/- 0.01 *vs* G93A-SOD1 mice = 0.20 +/- 0.05; +33%, $p < 0.05$) and at 120 days (WT mice = 0.14 +/- 0.06 *vs* G93A-SOD1 mice = 0.23+/- 0.03; +64%, p<0.001) (Fig. 3b).

Histological quantitative fluorescence results expressed in arbitrary units (AU) showed a significant decrease in YFP at earlier stages of the disease (80 days) (YFP mice = 20305 +/- 512 AU *vs* YFP, G93A-SOD1 mice = 18083 +/- 503 AU; -11 %, $p < 0.05$) and also in MBP levels: (YFP mice = 17486 +/- 2102 AU *vs* YFP, G93A-SOD1 mice = 12658 +/-1090 AU; -27%, $p < 0.01$) (Fig.4 a,b) . The YFP/MBP ratio in the YFP mice was 0.55 +/- 0.07 *vs* 0.56 +/-0.10 in the YFP, G93A-SOD1 mice. Note
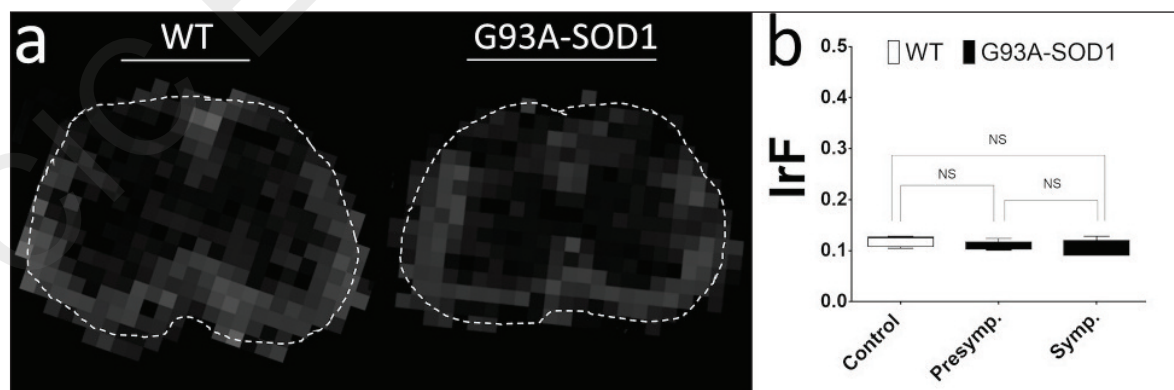

Figure 2 - Analysis of NODDI stationary water diffusion compartment in spinal cords of ALS mice.
a) Axial isotropic restricted fraction (IrF) maps from stationary models in lumbar spinal cords from *ex vivo* wild-type (WT) and ALS mice. To evaluate the integrity of the entire spinal cord tissue, the white matter and gray matter were included in the region of interest (dotted line). b) Statistical analysis between WT and presymptomatic and symptomatic ALS mice did not show any statistical difference (n=1 animal per group).

that correlative changes in YFP/MBP levels demonstrate a proportional decrease in axonal and WM oligodendrocyte markers during the pre-symptomatic and symptomatic stages of the disease (Fig. 4c). To validate the detection of changes in WM compartments by NODDI, we evaluated the intra-neurite or intra-cellular compartment (labeled by YFP maker) and the non-YFP space (extra-neurite or extra-cellular compartment) using thresholding methods to delineate and quantify the compartment changes in an approximately voxel sized region (100 x 100 µm²) (Fig. 5a). Thus, a statistically significant reduction (-22%, p < 0.01) in the total axonal areas was observed at 80 days (YFP mice = 3318 +/-84 µm² *vs* YFP, G93A-SOD1 mice = 2578 +/-189 µm²). Additionally, a significant expansion in the extra-axonal compartment was recorded in the early stages of the disease (YFP mice = 2629 +/-64 µm² *vs* YFP, G93A-SOD1 mice = 4504 +/-144 µm²; +71%, p < 0.01). A further decrease in axonal areas and an increase in the extra-neurite compartment were seen at later stages of the disease (120 days) (Fig. 5b).

Discussion

The application of MRI diffusion techniques to the investigation of neurodegenerative diseases has been increasing due to the development of magnets with stronger gradient strengths and increased spatial resolution (Wheeler-Kingshott et al., 2014). DTI has frequently been used in the search for potential biomarkers in ALS (de Albuquerque et al., 2017; Querin et al., 2017). However, considering the complexity of the biological tissue, using a mono-exponential decay diffusion model, such as DTI, to interrogate how different cell groups are affected in ALS becomes problematic. Thus, the development of new diffusion models allowing better representation of these changes is necessary for more accuracy and better assessment of the microstructural WM abnormalities (Rokem et al., 2015). NODDI, as a multi-shell MRI technique, simultaneously accounts for different diffusion compartments. For example, the intracellular compartment is modeled as infinitely long sticks whose collective orientations are characterized by a Watson distribution function. The second compartment is the extra-axonal compartment, assumed to be involved in fast water exchange with the extracellular space. This compartment is modeled as Gaussian anisotropic diffusion (i.e. tensor ellipsoids). The third compartment is modeled as Gaussian isotropic diffusion, which represents freely diffusing water.

In the last few years, NODDI methods have been not only been tested and

characterized in healthy subjects (Grussu et al., 2015; Nazeri et al., 2015) but also applied to the study of SC pathologies (Grussu et al., 2017) and just recently applied to brains from patients with ALS (Table I). The results presented in our study suggest that changes in diffusion are the result of pathological structural changes across multiple WM compartments at early stages of the disease (see, for example, Fig. 1).

Specifically, our NODDI analysis indicated that a compartmental redistribution occurs in the early stages of ALS, as represented by a decrease in NDI and increases in ODI and IVF (Fig. 3). Similar patterns of changes have also been observed in several neurodegenerative diseases, not only with predominant axonal impairment mechanisms (Colgan et al., 2016), but also in diseases with predominant myelin impairment (Schneider et al. 2017b). Overall, these results reflect the coexistent changes in both neurite content (NDI) and axonal complexity (ODI), due to a simultaneous degeneration of supporting cells located in the extra-neurite space.
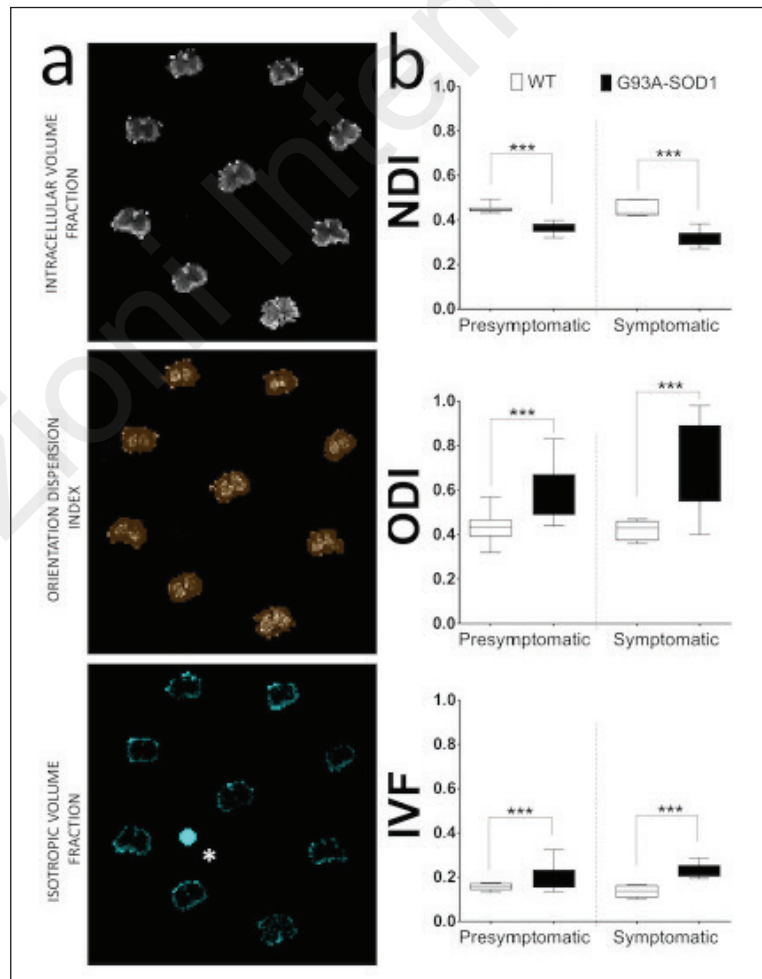

Figure 3 - Neurite orientation and density imaging detect presymptomatic axonal degeneration in the spinal cord of ALS mice.
a) NODDI outputs from one combined set of spinal cords. b) Analysis of 7 sections from WT mice (controls) and G93A-SOD1 mice (ALS mice) at the presymptomatic (day 80) and symptomatic (day 120) stages. (*) Note that the strong IVF signal from the capillary tube filled with water is used as a control. (*** p < 0.01). (n=5 mice per group, 7 axial slices per animal). Scale bar = 5 mm.

Table I - Summary of studies applying NODDI across different structural neurological diseases.

Year	Authors	Disease	Population	Diffusion b-values (s/mm2)	AT	Neural structures	ICVF	ODI	IVF
2018	Wu et al.	Mild TBI	Patients (n=19), controls (n=23)	250/1000/2000/4000/6250	21 min	Brain CCX (WM)	Decreased	NS	NS
2018	Parker et al.	YO Alzheimer's disease	Patients (n=38), controls (n=22)	300/700/2000	16 min	Brain CCX (GM)	Decreased	Decreased	NA
2018	Okita et al.	Cervical spondylotic myelopathy	Patients (n=25), controls (n=?)	500/1000/2000/3000	10 min	Spinal cord (WM)	Decreased	NS	NA
2018	Crombe et al.	Multiple sclerosis	EAE mice (n=18) / (n=18) (ev/iv)	1000/2000 & 1000/2700	38hs /2hs	Brain Hip. (GM)	NS	NS	NS
2018	Andica et al.	Parkinson's disease	Patients (n=29), controls (n=29)	1000/2000	13 min	Brain SN (WM)	Decreased	NS	Increased
2017	Bao et al. (*)	Amyotrophic lateral sclerosis	Patients (n=18), controls (n=14)	1000/2000	NA	Brain CST (WM)	Decrease	Increase	NS
2017	Song et al.	Wilson's disease	Patients (n=24), controls (n=25)	1000/2000	6.3 min	Brain BG (GM)	Decreased	Decreased	Increased
2017	Kamagata et al.	Parkinson's disease	Patients (n=30), controls (n=28)	1000/2000	13 min	Brain CCX (GM)	Decreased	Increased	NS
2017	Schneider et al.(b)	Multiple sclerosis	Patients (n=5), controls (n=5)	300/711/2000	15 min	Brain (WM)	Decreased	Increased	Increased
2017	Slattery et al.	YO Alzheimer's disease	Patients (n=23), controls (n=37)	300/700/2000	16 min	Brain (WM)	Decreased	Decrease	NS
2017	Schneider et al.(a)	Multiple sclerosis	Patients (n=5), controls (n=5)	300/711/2000	15 min	Brain (WM)	Decreased	Increased	NS
2017	Irie et al.	INP hydrocephalus	Patients (n=19), controls (n=12)	500/1000/1500/2000/2500	NA	Brain (WM)	Decreased	Decreased	NS
2017	Granber et al.	Multiple sclerosis	Patients (n=26), controls (n=24)	1000/5000	NA	Brain CCX (WM)	Decreased	Increased	NS
2017	By et al.	Multiple sclerosis	Patients (n=6), controls (n=8)	711/2855	18 min	Spinal cord (WM)	Decreased	Increased	NS
2016	Kini et al.	Subcortical heterotopia	Patient (n=1), control (n=1)	300/700/2000	NA	Brain (WM)	Decreased	NS	Decreased
2016	Kamagata et al.	Parkinson's disease	Patients (n=58), control (n=36)	1000/2000	13 min	Brain SN and BG (GM)	Decreased	Decreased	NS
2016	Colgan et al.	Alzheimer's disease	rTg4510 mice (n=5), WT mice (n=5)	1000/2000	NA	Brain (WM)	Decreased	Increased	NS
2016	Timmers et al.	Galactosemia	Patients (n=8), controls (n=8)	1000/2000	23 min	Brain CC (WM)	Decreased	Increased	NA
2015	Wen et al.	Brain tumor (glioma)	Patients (n=20), controls (n=5)	1000/2000	5 min	Brain (WM)	Decreased	Increased	Increased
2014	Adluru et al.	Stroke	Patients (n=2) vs contralateral side	500/1000/2000/5000	NA	Brain CC (WM)	Increased	Increased	Decreased
2014	Winston et al.	Cortical dysplasia & TS	Patients (n=5) vs contralateral side	700/2000	20 min	Brain (WM)	Decreased	NS	NA

Summary of recent findings from MRI studies using NODDI applied in Neurological Diseases.
Abbreviations: NODDI=neurite orientation dispersion and density imaging; AT=acquisition time; ICVF=intracellular volume fraction, ODI=orientation dispersion index; IVF=isotropic volume fraction; GM=gray matter; WM=white matter; WT=wild type; NA=not available; NS=not significant; CCX=cortex; Hip.=hippocampus; SN=substantia nigra; CST=cortical spinal tract; BG=basal ganglia; CC=corpus callosum; TBI= traumatic brain injury; YO=young onset; INP=idiopathic normal pressure; TS=tuberous sclerosis; ev=ex vivo; iv=in vivo; EAE=experimental autoimmune encephalitis; (*)=from conference proceedings, no publication record.

Thus, if the cellular and membrane volumes across glial cells in WM are reduced, these changes could increase the spacing between membranes and the extra-neurite space allowing additional water diffusion movements (IVF). Our use of histological fluorescent techniques for *ex vivo* YFP, G93A-SOD1 mice preparations highlighted early changes across different WM compartments (Fig. 4). Specifically, changes in axonal mass (shown by decreases in YFP) were concomitant with the deterioration of supporting cells (oligodendrocytes) as described previously (Nonneman et al., 2014). Moreover, the unchanged YFP/MBP ratios in control and disease groups showed that intra-axonal and extra-axonal compartments were simultaneously affected.

Overall, our results support the concept that structural changes in different cell compartments (each of them with unique diffusion properties) occur in the early stages of ALS (Fig. 5). Specifically, the substantial reduction of neurites indicated by the reduction in YFP fluorescence was in line with the reduction in the axonal volume fraction reported by NDI. Moreover, the increase in extra-axonal space and geometry complexity was mirrored by an increase in ODI and IVF (Table II). Thus, the work presented in this manuscript offers a new insight for understanding the biological nature of MRI diffusion changes during the early stages of this neurodegenerative disease and, in particular, how the degeneration of axonal and extra-axonal elements contributes to the early changes in WM microstructure and water diffusion changes captured by MRI signals. These results sug-

Table II - Early spinal cord white matter changes in MRI diffusion (NODDI) and histological findings in ALS mice.

MRI biomarkers (NODDI)	WM cellular markers	Histological alteration
ICVF ↓↓	YFP↓↓	Decrease in intra-axonal space (axonal degeneration)
	MBP ↓↓	Decrease in myelin content (oligodendrocyte degeneration)
ODI ↑↑	IVF ↑	Increase in extra-axonal space
		Increase in free water diffusion

Presymptomatic changes detected by NODDI can be associated with histological changes in different WM compartments. Abbreviations: ALS=amyotrophic lateral sclerosis; NODDI=neurite orientation dispersion and density imaging; ICVF=intracellular volume fraction; ODI=orientation dispersion index; IVF=isotropic volume fraction; WM=white matter; YFP=yellow fluorescent protein; MBP=myelin basic protein.
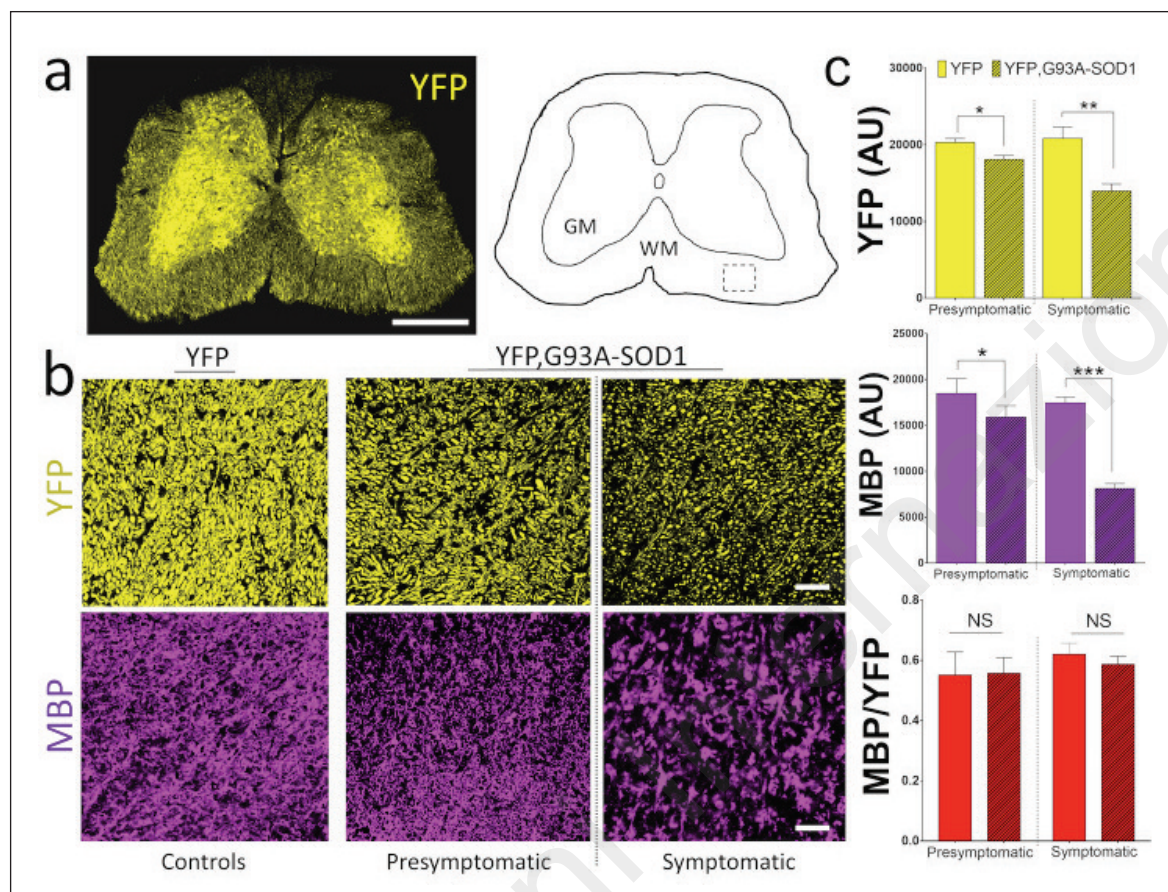
Figure 4 - Parallel reduction in yellow fluorescence protein (YFP) and myelin basic protein (MBP) levels in the spinal cord white matter of YFP, G93A-SOD1 mice.
a) Histological axial section from the lumbar region in YPF mice. Observe the clear differences between gray matter (GM) and white matter (WM). The region of interest was centered in the anterolateral WM funiculi (square). Scale bar = 1mm. b) Higher magnification in WM reveals individual axonal degeneration shown by YFP in lumbar spinal cords from pre-symptomatic (day 80) and symptomatic (day 120) YFP, G93A-SOD1 mice. Scale bar =10 microns. c) Quantitative analysis showed a significant decrease in YFP levels. A similar analysis by immunohistochemistry showed a significant reduction in presymptomatic MBP levels in the ALS mice. (* $p < 0.05$), (** $p < 0.01$), (*** $p < 0.01$), (n=4 mice per group).

gest that NODDI, as a multi-compartmental model, may have the ability to represent the microstructural WM changes in the context of ALS.

The use of NODDI in the context of ultra-high magnetic field MRI with extremely long scanning times has limited application in clinical scenarios. Nevertheless, shorter and optimized NODDI protocols are already used in clinical practice (Sepeherband et al., 2015; Schneider et al., 2017b; Ok ita et al., 2018; Parker et al., 2018) (Table I). Moreover, recent clinical studies have described the use of NODDI as a novel technique for the visual assessment of the underlying microstructural changes, possibly highlighting an increased inflammatory component, within lesions and potentially in normal-appearing WM (Caverzasi et al., 2016). However, some of these advantages of NODDI in detecting and characterizing changes in ALS are still limited due to the nature of the complex anomalous water diffusion process across an inhomogeneous and porous biological tissue, such as the CNS (Magin et al., 2011; Magin et al., 2013; Liang et al., 2016). In addition, the choice of acquisition parameters (e.g., b-values) was not optimized to detect multiple highly restricted diffusion compartments existing in an inhomogeneous tissue. Therefore, there is a need to employ multiple b-values in order to evaluate water diffusion in all the compartments likely to change when studying in vivo animal models of ALS (White et al., 2014; Fogarty et al., 2016).

In conclusion, the results of this *ex vivo* study suggest that NODDI can detect SC axonal degeneration at pre-symptomatic disease stages in ALS mice. Early changes in intracellular and extracellular diffusion compartments revealed by this model were validated by our histological studies, which provided further insights into the microstructural alterations detected by this imaging technique.

These results underscore the potential of multi-compartment diffusion models, using multi-shell acquisitions, to provide early imaging biomarkers for the detection and monitoring of patients with ALS.
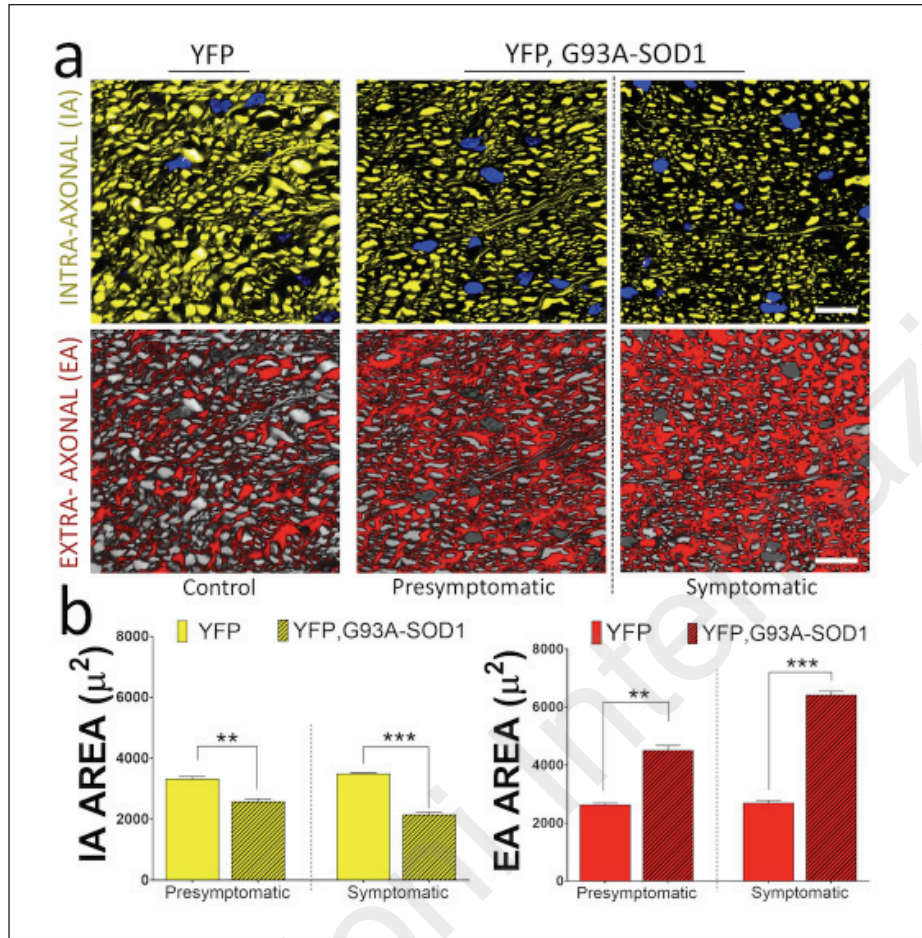
Figure 5 - Early abnormalities in MRI diffusion are associated with structural alterations and cellular changes in different histological compartments.
a) Evaluation of ventral white matter intra-axonal (intra-neurite, yellow) and extra-axonal (red) compartments in YFP, G93A-SOD1 mice at early and late stages of the disease. b) Quantitative analysis, which centered on the ventral fasciculus of the lumbar spinal cord shows, a significant decrease in the intra-axonal compartment measured by counting the total area of YFP and an increase in the extra-axonal compartment as early as day 80. Note that quantitative measurements from each compartment were calculated in areas of 100 x 100 microns^2 (similar to the voxel size used in our MRI experiments).Nuclei in blue stained with DAPI. Scale bar= 10 microns. (** $p < 0.01$), (*** $p < 0.01$), (n=4 mice per group).

References

Adluru G, Gur Y, Anderson JS, et al (2014). Assessment of white matter microstructure in stroke patients using NODDI. Conf Proc IEEE Eng Med Biol Soc 2014: 742-745.

Alexander AL, Lee JE, Lazar M, et al (2007). Diffusion tensor imaging of the brain. Neurotherapeutics no. 4: 316-329.

By S, Xu J, Box BA, et al (2017). Application and evaluation of NODDI in the cervical spinal cord of multiple sclerosis patients. Neuroimage Clin 15: 333-342.

Caverzasi E, Papinutto N, Castellano A, et al (2016). Neurite Orientation Dispersion and Density Imaging Color Maps to Characterize Brain Diffusion in Neurologic Disorders. J Neuroimaging 26: 494-498.

Colgan N, Siow B, O'Callaghan JM, et al (2016). Application of neurite orientation dispersion and density imaging (NODDI) to a tau pathology model of Alzheimer's disease. Neuroimage 125: 739-744.

Crombe A, Planche V, Raffard G, et al (2018). Deciphering the microstructure of hippocampal subfields with in vivo DTI and NODDI: Applications to experimental multiple sclerosis. Neuroimage 172: 357-368.

de Albuquerque M, Branco LM, Rezende TJ, et al (2017). Longitudinal evaluation of cerebral and spinal cord damage in Amyotrophic Lateral Sclerosis. Neuroimage Clin 14: 269-276.

Fogarty MJ, Klenowski PM, Lee JD, et al (2016). Cortical synaptic and dendritic spine abnormalities in a presymptomatic TDP-43 model of amyotrophic lateral sclerosis. Sci Rep 6: 37968.

Gatto RG, Chauhan M, Chauhan M (2015a). Anti-edema effects of rhEpo in experimental traumatic brain injury. Restor Neurol Neurosci 33: 927-941.

Gatto RG, Chu Y, Ye AQ, et al (2015b). Analysis of YFP(J16)-R6/2 reporter mice and postmortem brains reveals early pathology and increased vulnerability of callosal axons in Huntington's disease. Hum Mol Genet 24: 5285–5298.

Gatto RG, Li W, Magin RL (2018a). Diffusion tensor imaging identifies presymptomatic axonal degeneration in the spinal cord of ALS mice. Brain Res 1679: 7.

Gatto RG, Li W, Gao J, et al (2018b). In vivo Diffusion MRI Detects Early Changes in Spinal Cord Axonal Pathology in a Mouse Model of Amyotrophic Lateral Sclerosis. NMR in Biomedicine 8: e3954.

Gatto RG, Amin MY, Deyoung D, Hey M, Mareci TH, Magin RL. (2018c). Ultra-High Field Diffusion MRI Reveals Early Axonal Pathology in Spinal Cord of ALS mice. Transl Neurodegener 7:20.

Granberg T, Fan Q, Treaba CA, et al (2017). In vivo characterization of cortical and white matter neuroaxonal pathology in early multiple sclerosis. Brain 140: 2912-2926.

Grussu F, Schneider T, Zhang H, et al (2015). Neurite orientation dispersion and density imaging of the healthy cervical spinal cord in vivo. Neuroimage 111: 590-601.

Grussu F, Schneider T, Tur C, et al (2017). Neurite dispersion: a new marker of multiple sclerosis spinal cord pathology? Ann Clin Transl Neurol 4: 663-679.

Gurney ME (1994). Transgenic-mouse model of amyotrophic lateral sclerosis. N Engl J Med 331: 1721-1722.

Irie R, Tsuruta K, Hori M, et al (2017). Neurite orientation dispersion and density imaging for evaluation of corticospinal tract in idiopathic normal pressure hydrocephalus. Jpn J Radiol 35: 25-30.

Jelescu I, Budde M (2017). Design and validation of diffusion MRI models of white matter. Frontiers in Physics 5: 18.

Kaden E, Kelm ND, Carson RP, et al (2016). Multi-compartment microscopic diffusion imaging. Neuroimage 139: 346-359.

Kamagata K, Hatano T, Okuzumi A, et al (2016). Neurite orientation dispersion and density imaging in the substantia nigra in idiopathic Parkinson disease. Eur Radiol 26: 2567-2577.

Kini LG, Nasrallah IM, Coto C, et al (2016). Advanced structural multimodal imaging of a patient with subcortical band heterotopia. Epilepsia Open 1: 152-155.

Kodiweera C, Alexander AL, Harezlak J, et al (2016). Age effects and sex differences in human brain white matter of young to middle-aged adults: A DTI, NODDI, and q-space study. Neuroimage 128: 180-192.

Liang Y, Ye AQ, Chen W, et al (2016). A fractal derivative model for the characterization of anomalous diffusion in magnetic resonance imaging. Commun Nonlinear Sci Numer Simulat 39: 529-537.

Magin RL, Akpa BS, Neuberger T, et al (2011). Fractional order analysis of sephadex gel structures: NMR measurements reflecting anomalous diffusion. Commun Nonlinear Sci Numer Simul 16: 4581-4587.

Magin RL, Ingo C, Colon-Perez L, et al (2013). Characterization of anomalous diffusion in porous biological tissues using fractional order derivatives and entropy. Microporous Mesoporous Mater 178: 39-43.

Magin R (2017). Models of diffusion signal decay in magnetic resonance imaging: capturing complexity. Concepts Magn Reson Part A. (e21401): 15.

Mancuso R, Olivan S, Mancera P, et al (2012). Effect of genetic background on onset and disease progression in the SOD1-G93A model of amyotrophic lateral sclerosis. Amyotroph Lateral Scler 13: 302-310.

Morfini GA, Bosco DA, Brown H, et al (2013). Inhibition of fast axonal transport by pathogenic SOD1 involves activation of p38 MAP kinase. PLoS One 8: e65235.

Nair G, Carew JD, Usher S, et al (2010). Diffusion tensor imaging reveals regional differences in the cervical spinal cord in amyotrophic lateral sclerosis. Neuroimage 53: 576-583.

Nazeri A, Chakravarty MM, Rotenberg DJ, et al (2015). Functional consequences of neurite orientation dispersion and density in humans across the adult lifespan. J Neurosci 35: 1753-1762.

Nonneman A, Robberecht W, Van Den Bosch L (2014). The role of oligodendroglial dysfunction in amyotrophic lateral sclerosis. Neurodegener Dis Manag 4: 223-239.

Okita G, Ohba T, Takamura T, et al (2018). Application of neurite orientation dispersion and density imaging or diffusion tensor imaging to quantify the severity of cervical spondylotic myelopathy and to assess postoperative neurologic recovery. Spine J 18: 268-275.

Orsini M, Oliveira AB, Nascimento OJ, et al (2015). Amyotrophic lateral sclerosis: new perpectives and update. Neurol Int 7: 5885.

Parker TD, Slattery CF, Zhang J, et al (2018). Cortical microstructure in young onset Alzheimer's disease using neurite orientation dispersion and density imaging. Hum Brain Mapp 39: 3005-3017.

Querin G, El Mendili MM, Lenglet T, et al (2017). Spinal cord multi-parametric magnetic resonance imaging for survival prediction in amyotrophic lateral sclerosis. Eur J Neurol 24: 1040-1046.

Redler RL, Dokholyan NV (2012). The complex molecular biology of amyotrophic lateral sclerosis (ALS). Prog Mol Biol Transl Sci 107: 215-262.

Rokem A, Yeatman JD, Pestilli F, et al (2015). Correction: evaluating the accuracy of diffusion MRI models in white matter. PLoS One 10: e0139150.

Sato K, Kerever A, Kamagata K, et al (2017). Understanding microstructure of the brain by comparison of neurite orientation dispersion and density imaging (NODDI) with transparent mouse brain. Acta Radiol Open no. 6: 1-4.

Schneider CA, Rasband WS, Eliceiri KW (2012). NIH Image to ImageJ: 25 years of image analysis. Nat Methods 9: 671-675.

Schneider T, Brownlee W, Zhang H, et al (2017). Sensitivity of multi-shell NODDI to multiple sclerosis white matter changes: a pilot study. Funct Neurol 32: 97-101.

Sepehrband F, Clark KA, Ullmann JF, et al (2015). Brain tissue compartment density estimated using diffusion-weighted MRI yields tissue parameters consistent with histology. Hum Brain Mapp 36: 3687-3702.

Slattery CF, Zhang J, Paterson RW, et al (2017). ApoE influences regional white-matter axonal density loss in Alzheimer's disease. Neurobiol Aging 57: 8-17.

Song YK, Li XB, Huang XL, et al (2017). A study of neurite orientation dispersion and density imaging in wilson's disease. J Magn Reson Imaging 48: 423-430.

Timmers I, Zhang H, Bastiani M, et al (2015). White matter microstructure pathology in classic galactosemia revealed by neurite orientation dispersion and density imaging. J Inherit Metab Dis 38: 295-304.

Watson C, Paxinos G, Kayalioglu G (2008). The spinal cord: a Christopher and Dana Reeve Foundation text and atlas. 1st Edition, Academic Press, London.

Wen Q, Kelley DA, Banerjee S, et al (2015). Clinically feasible NODDI characterization of glioma using multiband EPI at 7 T. Neuroimage Clin 9: 291-299.

Wheeler-Kingshott CA, Stroman PW, Schwab JM, et al (2014). The current state-of-the-art of spinal cord imaging: applications. Neuroimage 84: 1082-1093.

White NS, McDonald C, Farid N, et al (2014). Diffusion-weighted imaging in cancer: physical foundations and applications of restriction spectrum imaging. Cancer Res 74: 4638-4652.

Wijesekera LC, Leigh PN (2009). Amyotrophic lateral sclerosis. Orphanet J Rare Dis 4: 3.

Winston GP, Micallef C, Symms MR, et al (2014). Advanced diffusion imaging sequences could aid assessing patients with focal cortical dysplasia and epilepsy. Epilepsy Res 108: 336-339.

Wu YC, Mustafi SM, Harezlak J, et al (2018). Hybrid diffusion imaging in mild traumatic brain injury. J Neurotrauma 35: 1-14.

Zhang H, Schneider T, Wheeler-Kingshott CA, et al (2012). NODDI: practical in vivo neurite orientation dispersion and density imaging of the human brain. Neuroimage 61: 1000-1016.